Journal of
Applied Crystallography

ISSN 0021-8898

Received 27 July 2005
Accepted 3 October 2005

A refractive focusing lens system for small-angle neutron scattering

D. F. R. Mildner,* B. Hammouda and S. R. Kline

National Institute of Standards and Technology, Gaithersburg, MD 20899, USA. Correspondence e-mail: david.mildner@nist.gov

Simple neutron optics measurements have been performed using optical-quality concave lenses as a function of neutron wavelength on a 30 m SANS instrument. The variation in the width of the beam spot on the detector at wavelengths different from the focused condition has been observed. The movement of the beam on the detector when the centerline of the lens combination is shifted from the incident-beam centerline has also been observed. These results are compared with theoretical predictions.

1. Introduction

Small-angle neutron scattering (SANS) is a valuable technique for materials characterization from the near nanometer to the near micrometer size range. Both the long-wavelength neutrons and the long flight paths necessary to resolve small scattering wavevectors, and therefore large (near micrometer) size scales within the sample, result in low intensity at the detector. In fact, neutron scattering in general is characterized by limited flux on the sample. Various authors have made efforts to focus long wavelength neutrons, in particular to improve the resolution of SANS measurements relative to pinhole collimation. Focusing also reduces the minimum measurable scattering vector and increases the neutron intensity on the sample. Littrell (2004) has summarized various methods for focusing, including multiple confocal pinhole apertures (for example, Glinka *et al.*, 1986), focusing mirrors (for example, Kentzinger *et al.*, 2004) and converging lenses. Eskildsen *et al.* (1998) and Choi *et al.* (2000) have explored the use of single-crystal compound refractive lenses, based on an earlier arrangement of Gähler *et al.* (1980). Other efforts have used a concave Fresnel compound refractive lens (Oku *et al.*, 2001; Adachi *et al.*, 2003). Finally, the magnetic superconducting lens is another method for focusing cold neutrons (Suzuki *et al.*, 2003; Shimizu *et al.*, 2004; Oku *et al.*, 2004).

The use of both long-wavelength neutrons and long flight paths results in the transmitted beam falling under the influence of gravity by an amount that is wavelength dependent, giving a further contribution to the resolution (Boothroyd, 1989). This smearing results in an oval shape to the neutron beam spot on the detector, and corrections for this gravity effect are rarely performed in normal SANS measurements, making long wavelengths less useful. A prism can compensate for the chromatic aberration caused by gravity because the refractive index for neutrons has similar wavelength dependence to gravity. An antigravity device has been demonstrated by Forgan & Cubitt (1998) using single-crystal prisms such that the transmitted beam is restored to the instrument centerline defined by the source and sample apertures. Furthermore, others have studied both the magnetic prism (Badurek *et al.*, 1979) and the compound refractive prism made of single-crystal elements (Adachi *et al.*, 2002).

Neutron lenses have been in use on SANS instruments for a few years. Our 30 m instrument on the NG3 guide (Glinka *et al.*, 1998) has been equipped with two sets of lens systems, each using concave MgF_2 lenses of 25 mm curvature radius, 25 mm cylinder diameter and 7.24 mm thickness. These are 0.5 mm in thickness at the center in order to improve neutron transmission. (Appendix *A* gives the calculation of the transmission.) The first system uses 30 such lenses at a neutron wavelength of 8.4 Å, and the second uses seven lenses at a wavelength of 17.2 Å. Both devices are included in the last section of the pre-sample (evacuated) collimation flight path and their movement is computer controlled for routine use.

The use of prisms to correct for chromatic aberration suffers on account of the transmission losses that are high and vary with position across the beam. We wish to test the concept of raising the lens system from the spectrometer axis in order to correct for gravity and restore the beam to the axis at the detector. Moreover, obtaining an analytic basis for understanding neutron focusing with lenses might help in making corrections for the smearing. Here, we use the seven-lens system for our analysis.

2. Lens basic equations

The focal distance f for a set of N concave lenses of radius of curvature r is given by (Sears, 1989)

$$f = r/2N(1-n), \tag{1}$$

where the index of refraction n is related to the average bound coherent scattering length b_c, the atomic number density ρ, and the neutron wavelength λ by

$$n = 1 - \rho b_c \lambda^2/2\pi. \tag{2}$$

In the case of the single-crystal MgF_2 lenses used here, r = 25 mm, and $\rho b_c/\pi = 1.632 \times 10^{-6}$ Å^{-2}, so that the index of refraction varies as $n = 1 - (0.816 \times 10^{-6})\lambda^2$ (Å). A basic geometric optics equation relates the focal length f to the distance L_1, between the source aperture and the lens center position, and the lens-to-image distance L_2 as

$$1/f = 1/L_1 + 1/L_2. \quad (3)$$

The seven-lens set is placed in the sample position of the NG-3 SANS instrument and has a length of 51 mm. The distance L_1 is 16.14 m, and the distance L_2 between the lens center position and the two-dimensional detector is 13.19 m. From equation (3), the focal length of the lens combination is required to be 7.26 m. Hence this arrangement results in an optimum wavelength for the seven-lens combination of 17.32 Å for our experimental arrangement, though there is chromatic aberration to blur the results.

3. Measurements

Measurements were performed inside the sample chamber with an aperture of radius R_2 = 6.35 mm placed 100 mm before the lens system center. In normal lens use, this aperture is larger. One of the advantages in using focusing lenses instead of the standard converging pinhole collimation is that for $L_1 = L_2$ the image spot size (beam stop) is uniform, equal in size to the source aperture and independent of the lens aperture size (instead of having a triangular shape with a base width twice that of the source for the standard collimation.) A larger aperture of diameter 22 mm was placed immediately after the seven-lens system in order to reduce the background from stray neutrons.

We have performed a series of measurements through the lens system at different wavelengths between 6 and 20 Å. The multidisk neutron velocity selector (Hammouda, 1992) of the instrument has a measured wavelength band width $\Delta\lambda/\lambda$ = 0.1199 (32) at λ_0 = 17.2 Å, where $\Delta\lambda$ is the FWHM (full width at half-maximum) of the assumed triangular form of the neutron wavelength distribution around the nominal wavelength. (We ignore any variation in the neutron spectrum.) We record both the position (x, y) of the center of the beam spot on the detector and its width, as determined by the FWHM, in each of the horizontal x and vertical y directions. The two-dimensional detector has pixel sizes of 5 by 5 mm. A cut of width 2 pixels is made across the center of the beam spot, and the resulting profile is fitted to a Gaussian to obtain the FWHM = 2.35σ, where σ^2 is the variance of the transverse spatial distribution of the beam intensity in each direction.

Firstly, measurements were taken without the lens system in place. Then, the focal condition was determined by varying the neutron wavelength with the lens system in place. Using the optimum focusing wavelength, the lens system was raised using shims of thickness 0.533 mm each, in order to assess the effect of controlled vertical shifts on both the beam center and the beam width. Horizontal shifts of the lens system were also investigated. Finally, the size of the beam-defining aperture (just before the lens system) was varied. In each case, the experimental results are presented together with the analytic equations for the beam width at the detector as a function of wavelength that have been derived in Appendix *B*, assuming the thin-lens approximation. This is valid because the length (51 mm) of the compound refractive lens is much shorter than its focal length (Pantell *et al.*, 2003). However, the averaging along a thin strip rather than across the entire beam spot increases the variances caused by the beam apertures by a factor of 4/3. Furthermore, there will also be some broadening caused by the finite size of the detector pixels, with standard deviation of the detector pixel size, $\Delta x/(12)^{1/2} = \Delta y/(12)^{1/2}$ = 1.443 mm.

The collimation for the measurements is a source aperture of radius R_1 = 7.15 mm, and an aperture of radius R_2 = 6.35 mm placed in front of the lens set. Some useful values are $(L_2/L_1)(R_1/2)$ = 2.922 mm and $(1 + L_2/L_1)(R_2/2)$ = 5.770 mm. The beam falls under gravity by an amount $A\lambda^2$, where the calculated value of $A = L_2(L_1 + L_2)gm^2/(2h^2)$ = 0.1189 mm Å^{-2}, where g = 981 m s^{-1} is the acceleration due to gravity, h/m = 3995 Å m s^{-1}, m is the mass of the neutron and h is Planck's constant. Other useful values are $(2/3)^{1/2}A\lambda_0{}^2(\Delta\lambda/\lambda)$ = 3.444 (92) mm and $(1 + L_2/L_1)(R_2/2) \times (2/3)^{1/2}(\Delta\lambda/\lambda)$ = 0.565 (15) mm.

3.1. Measurements as a function of wavelength with no lenses in place

We first make measurements without the lens so that the distribution of transmitted neutrons on the detector is determined by the collimation of the system. The x position of the beam obviously does not change with wavelength, whereas the y position decreases because of gravity as $y = y_0 - A\lambda^2$. Experimentally we find A = 0.118 (1) mm Å^{-2}, in agreement with theory. More accurately this becomes $y = y_0 - A\lambda^2[1 + (1/6)(\Delta\lambda/\lambda)^2]$ because of the chromaticity of the beam; a negligible difference of 0.4%.

The width of the beam spot in the horizontal x direction is also independent of the wavelength. This is found experimentally with poor statistics, with a constant standard deviation σ_x = 7.84 (3) mm. This should be compared with the expected variance of

$$\sigma_x^2 = (L_2/L_1)^2(R_1/3^{1/2})^2 + (1 + L_2/L_1)^2(R_2/3^{1/2})^2 + (\Delta x)^2/12, \quad (4)$$

which gives a value of σ_x = 7.61 mm. In the vertical direction there is an additional factor from the chromatic nature of the beam. Consequently, the expected value of the variance of the beam width in the y direction is given by

$$\sigma_y^2 = (L_2/L_1)^2(R_1/3^{1/2})^2 + (1 + L_2/L_1)^2(R_2/3^{1/2})^2 + (\Delta y)^2/12 + (2/3)A^2\lambda^4(\Delta\lambda/\lambda)^2. \quad (5)$$

Fig. 1 shows the results of these measurements as a function of wavelength. The fit to the data of the form $(\sigma_{y0}^2 + c^2\lambda^4)^{1/2}$ gives σ_{y0} = 7.94 (2) mm and A = 0.108 (4) mm Å^{-2}. Error bars in the figure represent the standard deviation of the fitted FWHM for each point. The large discrepancy in the fitted value of A

may arise because there are so few pixels in the small beam spot that contribute to each data point, and as a result of systematic error in the measurement of the incident-beam wavelength spread $\Delta\lambda/\lambda$.

3.2. Measurements as a function of wavelength with the lens system in place

Fig. 2 shows the variation in the coordinates (x, y) of the beam spot center as a function of neutron wavelength λ after transmission through the lens combination, showing the effect of gravity on the vertical coordinate. As before, the x position of the beam does not change with wavelength, whereas the y position is decreased by gravity as $y = y_0 - A\lambda^2$. Experimentally we find $A = 0.121\ (1)$ mm Å^{-2}, close to the expected value. Taking into account the chromaticity of the beam this equation becomes $y = y_0 - A\lambda^2[1 + (1/6)(\Delta\lambda/\lambda)^2]$. These equations have a negligible difference of 0.4%.

Fig. 3 shows the variation of the width of the beam spot on the detector in the two orthogonal directions as a function of neutron wavelength λ after transmission through the lens combination. With the lenses present the width of the beam spot is no longer independent of wavelength because it is only at $\lambda = \lambda_0$ that the beam is focused onto the detector plane. We show in Appendix *B* that the expected value of the variance of the beam width in the horizontal x direction is given by

$$\sigma_x^2 = (L_2/L_1)^2(R_1/3^{1/2})^2 + (1 + L_2/L_1)^2(R_2/3^{1/2})^2\left[1 - (\lambda/\lambda_0)^2\right]^2 + (\Delta x)^2/12. \quad (6)$$

Experimentally the data follow this form. The fit to the data by an expression of the functional form $\sigma_x = \{c_1^2 + c_2^2[1 - (\lambda/\lambda_0)^2]^2\}^{1/2}$, with three adjustable parameters, gives $c_1 = 3.91\ (5)$ mm, $c_2 = 6.50\ (12)$ mm, and $\lambda_0 = 16.94\ (17)$ Å. Expression (6) clearly has a minimum at $\lambda = \lambda_0$. More strictly, taking into account the wavelength distribution of the incident beam, this expression is a little more complicated, such that the variance at $\lambda = \lambda_0$ is given by

$$\sigma_x^2 = (L_2/L_1)^2(R_1/3^{1/2})^2 + (1 + L_2/L_1)^2(R_2/3^{1/2})^2(2/3)(\Delta\lambda/\lambda)^2 + (\Delta x)^2/12, \quad (7)$$

with the minimum occurring at $\lambda = 0.991\lambda_0$.

Again in the vertical direction there is an additional factor from the chromatic nature of the beam. Consequently, the expected value of the variance of the beam width in the y direction is given by

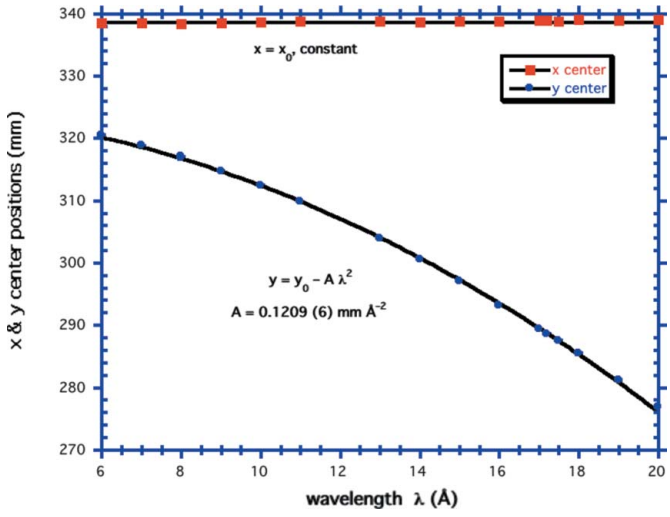

Figure 2
The coordinates (x, y) of the beam spot center as a function of neutron wavelength λ after transmission through the lens combination, showing the effect of gravity of the vertical coordinate.

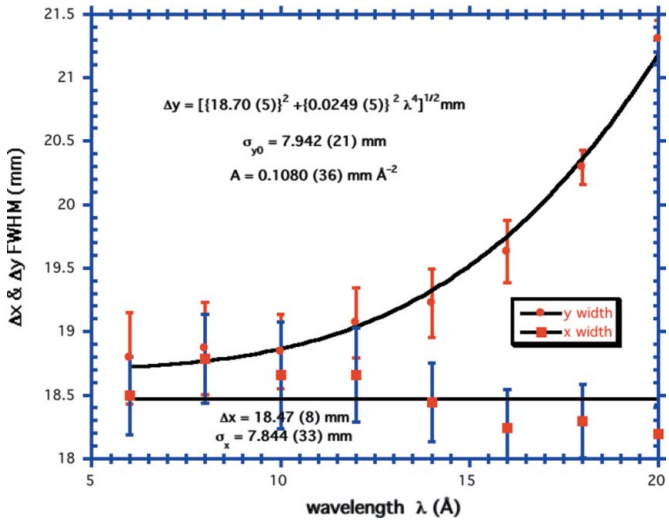

Figure 1
The widths of the beam spot on the detector as a function of wavelength λ after transmission through the two apertures but with no lenses in place. The x width remains constant with a standard deviation $\sigma_x = 7.84\ (3)$ mm, while the standard deviation of the y width increases approximately as $(\sigma_{y0}^2 + c^2\lambda^4)^{1/2}$, with $\sigma_{y0} = 7.94\ (2)$ mm and $c = 0.0105\ (2)$ mm Å^{-2}.

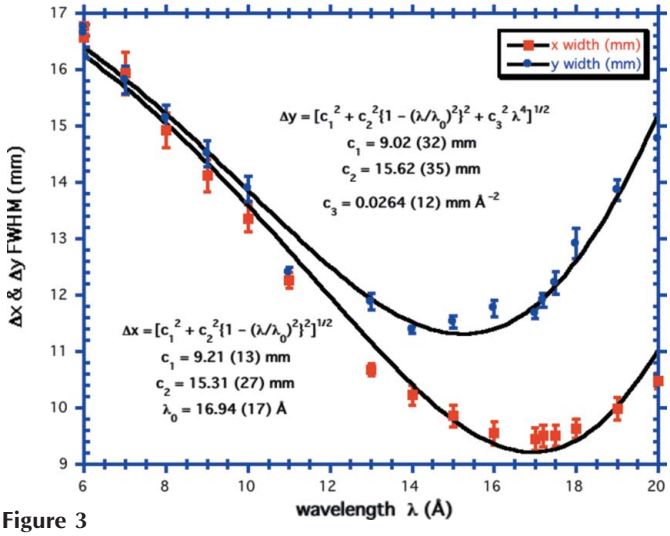

Figure 3
The width of the beam spot on the detector in the two orthogonal directions as a function of neutron wavelength λ after transmission through the lens combination. The data follow the expected form, with the minimum width in the horizontal direction occurring at $\lambda = \lambda_0$. The width in the vertical direction is always greater on account of the chromatic aberration, and the minimum occurs at a shorter wavelength.

$$\sigma_y^2 = (L_2/L_1)^2(R_1/3^{1/2})^2 + \{(1 + L_2/L_1)^2(R_2/3^{1/2})^2 \times \left[1 - (\lambda/\lambda_0)^2\right]^2\} + (\Delta y)^2/12 + (2/3)A^2\lambda^4(\Delta\lambda/\lambda)^2. \quad (8)$$

Experimentally the data follow this form. The fit to the data of the expression for the standard deviation, $\sigma_y = \{c_1^2 + c_2^2[1 - (\lambda/\lambda_0)^2]^2 + c_3^2\lambda^4\}^{1/2}$ using $\lambda_0 = 16.94$ Å, gives $c_1 = 3.83$ (14) mm, $c_2 = 6.63$ (15) mm and $c_3 = 0.0112$ (5) mm Å^{-2}, such that $A = 0.114$ (6) mm Å^{-2}.

This expression has a minimum at approximately $\lambda = \lambda_0\{1 + (2/3)A^2\lambda_0^4(\Delta\lambda/\lambda)^2/[(1 + L_2/L_1)^2(R_2/3^{1/2})^2]\}^{-1/2}$; that is, at a wavelength that is less than λ_0. Theoretically the minimum should occur at $\lambda = \lambda_0[1 + (3.44/6.66)^2]^{-1/2} = 15.3$ Å. Fig. 3 shows that the experimentally measured minimum occurs at 15.2 Å. The vertical width is always greater than the horizontal width on account of the extra chromatic aberration introduced through the gravitational contribution.

3.3. Measurements at λ_0 = 17.2 Å as the lens system is raised vertically

We can partially compensate for the fall caused by gravity by raising the lens system. We have therefore made further measurements with the lens combination slightly off-center at a wavelength $\lambda_0 = 17.2$ Å close to that corresponding to a minimum in the x width of the beam spot, when the detector is at the focal position for the two path lengths and the particular wavelength. We use a series of shims to raise the lens system above the beam centerline defined by the collimation. Fig. 4 shows the change in the beam spot position as a function of the number of shims. As expected this has no effect on the horizontal x position of the beam spot. However, the vertical y position increases with shim thickness w as $y = y_0 - A\lambda_0^2 + w(1 + L_2/L_1)$; that is, the y position moves up as the lens system is raised. This is shown experimentally, with $dy/dw = 1.96$ (2). We would expect $dy/dw = (1 + L_2/L_1) = 1.82$.

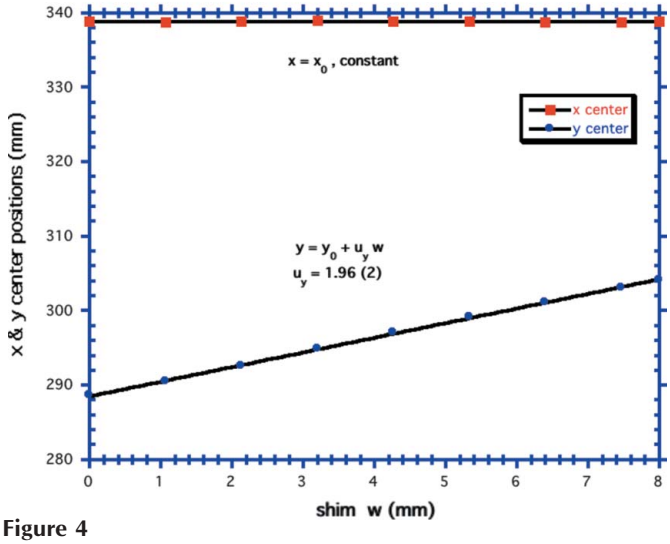

Figure 4
The coordinates (x, y) of the beam spot center as a function of the number of shims of thickness 0.533 mm used to shift the lens centerline vertically upwards. The x coordinate remains constant, while the y coordinate changes linearly.

Fig. 5 shows the width of the beam spot as a function of the number of shims. As expected, the width of the beam spot in the horizontal x direction is independent of shim thickness, with a constant $\sigma_x = 4.04$ (1) mm. This should be compared with the value of 3.72 mm obtained from equation (7). In the vertical y direction, however, the FWHM appears to decrease nonlinearly as the shim height w is increased. The expected beam width is given by

$$\sigma_y^2 = (L_2/L_1)^2(R_1/3^{1/2})^2 + (1 + L_2/L_1)^2(R_2/3^{1/2})^2(2/3)(\Delta\lambda/\lambda)^2 + (\Delta y)^2/12 + (2/3)A^2\lambda_0^4(\Delta\lambda/\lambda)^2\left[1 - 2(1 + L_2/L_1)w/(A\lambda_0^2)\right]. \quad (9)$$

Over the experimental range this is seen as an approximate linear decrease with shim thickness w. Certainly experiment shows a decrease, though the statistics are poor. Unfortunately, the four largest shim thicknesses used cause the lens to be partially occluded by the lens aperture, so that the data for shim widths of 5 mm or greater do not apply. However the width $\sigma_y = 5.07$ (5) mm at $w = 0$ is equal to the expected value of 5.07 mm.

3.4. Measurements at λ_0 = 17.2 Å as the lens system is shifted horizontally

The horizontal beam width is a better measure of the spot size at the detector because it is not affected by gravity. We have therefore made similar measurements at a wavelength $\lambda_0 = 17.2$ Å with a series of shims to shift the lens horizontally relative to the beam centerline defined by the collimation. Fig. 6 shows the change in the beam spot position as a function of the number of shims. The horizontal x position of the beam spot moves linearly in the opposite direction to the shim as $x =$

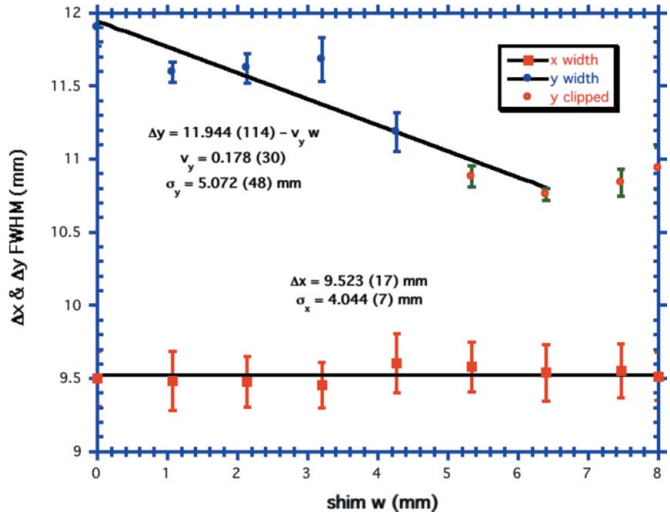

Figure 5
The widths of the beam spot on the detector as a function of the number of shims of thickness 0.533 mm used to shift the lens centerline vertically upwards. The x width remains constant, with a standard deviation $\sigma_x = 4.04$ (1) mm, while the y width, with $\sigma_{y0} = 5.07$ (5) mm, decreases approximately linearly. The four greatest numbers of shims cause the lens to be partially occluded by the lens aperture.

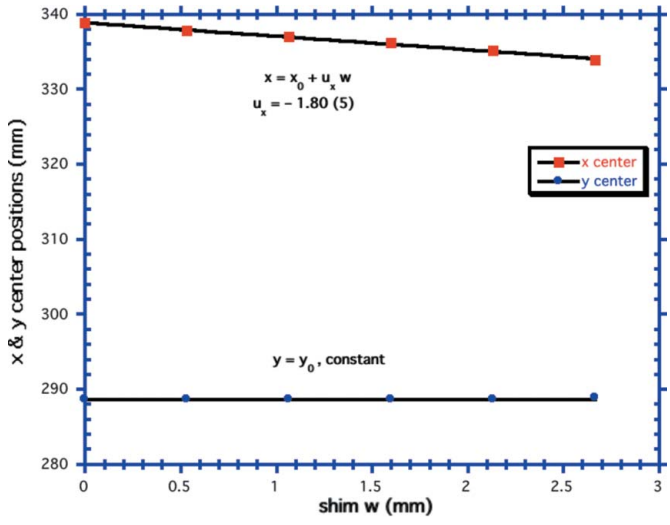

Figure 6
The coordinates (x, y) of the beam spot center as a function of the number of shims of thickness 0.533 mm used to shift the lens centerline horizontally. The y coordinate remains constant, while the x coordinate changes linearly. The beam widths also remain constant in both directions.

$x_0 - w(1 + L_2/L_1)$. This trend is shown experimentally, with $dx/dw = -1.80$ (5). We would expect $dx/dw = -(1 + L_2/L_1) = -1.82$. Correspondingly, as expected, this has no effect on the vertical y position of the beam spot.

We expect the beam width in the horizontal direction to be independent of the horizontal shift of the lens. Experimentally we find that the width is a constant with $\sigma_x = 3.88$ (6) mm, though with poor statistics, to be compared with the expected value of 3.72 mm from equation (7). In the vertical y direction, we also find that the width is independent of the horizontal shift of the lens and is constant with $\sigma_y = 5.03$ (1) mm, to be compared with the expected value of 5.07 mm.

3.5. Measurements at λ_0 = 17.2 Å as the lens aperture is varied

We should expect that the resolution of a SANS measurement has a very small dependence on the sample aperture size (Mildner, 2005) at the optimum wavelength for focusing, whereas the intensity on sample increases as the square of R_2, which is the purpose of the focusing lens. Measurements were taken with four different sizes of the beam-defining aperture (immediately before the lens system) with the radius R_2 between 4.76 and 9.5 mm. The centers of the beam spot remain unchanged, of course, though the total intensity in the pixels in each of the directional cuts through the beam center on the detector increases linearly with the aperture radius. The widths of the beam spots in each direction should have the same, very small dependence on R_2 given by (7). However, we find that the widths of the beam spots in each direction have a different variation. The width in the x direction has the expected slight increase with R_2, whereas the width in the y direction surprisingly has a slight decrease, though the changes in each direction are very small. This effect is probably an artifact of the analysis because the relative increase in the width in the x direction is greater than that in the y direction, so that the beam outline becomes less oval as the lens aperture is increased.

Table 1
Comparison of experimentally measured and expected standard deviations of beam widths in the x (horizontal) and y (vertical) directions, with the wavelength-dependent gravity term in the y direction determined separately at $\lambda_0 = 17.2$ Å, for the various measurements; also given is the ratio of the measured and expected standard deviations.

	Measured σ (mm)	Theoretical σ (mm)	Ratio
(1) No lenses [equations (4) and (5)]			
x	7.844 (33)	7.604	1.03
y	7.942 (21)	7.604	1.04
Gravity term $(2/3)^{1/2}A\lambda_0^2(\Delta\lambda/\lambda)$ (at $\lambda = \lambda_0$)			
y	3.123 (68)	3.444 (92)	0.91
(2) With lenses [equations (6) and (8)]			
R_1 term			
x	3.912 (53)	3.666	1.07
y	3.830 (137)	3.666	1.04
R_2 term			
x	6.501 (116)	6.662	0.98
y	6.633 (150)	6.662	1.00
Gravity term $(2/3)^{1/2}A\lambda_0^2(\Delta\lambda/\lambda)$ (at $\lambda = \lambda_0$)			
y	3.319 (151)	3.444 (92)	0.96
(3) y shim (at $\lambda = \lambda_0$ and $w = 0$)			
x	4.044 (7)	3.723	1.09
y	5.072 (48)	5.071	1.00
(4) x shim (at $\lambda = \lambda_0$ and $w = 0$)			
x	3.878 (56)	3.723	1.04
y	5.025 (5)	5.071	0.99

4. Discussion

We have found that the variation in the position of the beam spot on the detector as a function of wavelength and of small vertical and horizontal shifts of the lens system is as expected. Fig. 3 indicates the general trends of the beam width in the two directions as a function of λ. Table 1 summarizes the results of the beam widths and indicates the slightly narrower than expected vertical widths at λ_0. We believe that the major source of error in our measurements of the beam width at each wavelength is the result of having so few data points in the Gaussian fit to the beam spot. The fit for the horizontal beam width involves only four data points and generally is not as good as that for the vertical beam width, which involves six data points. At the focusing wavelength λ_0, the beam spot becomes oval, with a ratio of major-to-minor axes of about 1.6.

We find that around the focusing wavelength the experimental widths in the vertical direction are narrower than expected, in contrast to the horizontal direction. Fig. 7 shows a comparison between the experimentally fitted standard deviation of the beam spot in the two directions and the prediction [equations (7) and (8)] as a function of wavelength. At short wavelengths the beam spot is symmetric. For example, in Fig. 3 the FWHM at 6 Å in both directions is about 16.5 mm. At $\lambda_0 = 17.2$ Å, the vertical FWHM is about 12 mm, whereas the horizontal FWHM is about 9.5 mm. Therefore, the 2 pixel-wide (10 mm) fit of the beam profile to a Gaussian

Table 2
Expressions averaged over the wavelength distribution of the incident beam, assuming (i) a triangular distribution of FWHM $\Delta\lambda$, and (ii) a Gaussian distribution of FWHM = $2.35\sigma_\lambda$, where σ_λ is the standard deviation of the distribution.

Quantity	Quantity averaged over triangular distribution	Quantity averaged over Gaussian distribution
λ^2	$\lambda^2[1 + (1/6)(\Delta\lambda/\lambda)^2]$	$\lambda^2[1 + (\sigma_\lambda/\lambda)^2]$
λ^4	$\lambda^4[1 + (\Delta\lambda/\lambda)^2 + (1/15)(\Delta\lambda/\lambda)^4]$	$\lambda^4[1 + 6(\sigma_\lambda/\lambda)^2 + 3(\sigma_\lambda/\lambda)^4]$
$[1 - (\lambda/\lambda_0)^2]^2$	$[1 - (\lambda/\lambda_0)^2]^2 + (\Delta\lambda/\lambda)^2(\lambda/\lambda_0)^2 \times[(\lambda/\lambda_0)^2 - 1/3] + (1/15)(\Delta\lambda/\lambda)^4(\lambda/\lambda_0)^4$	$[1 - (\lambda/\lambda_0)^2]^2 + 6(\sigma_\lambda/\lambda)^2(\lambda/\lambda_0)^2 \times[(\lambda/\lambda_0)^2 - 1/3] + 3(\sigma_\lambda/\lambda)^4(\lambda/\lambda_0)^4$
σ_g^2	$(2/3)A^2\lambda^4(\Delta\lambda/\lambda)^2[1 + (7/120)(\Delta\lambda/\lambda)^2]$	$4A^2\lambda^4(\sigma_\lambda/\lambda)^2[1 + (1/2)(\sigma_\lambda/\lambda)^2]$

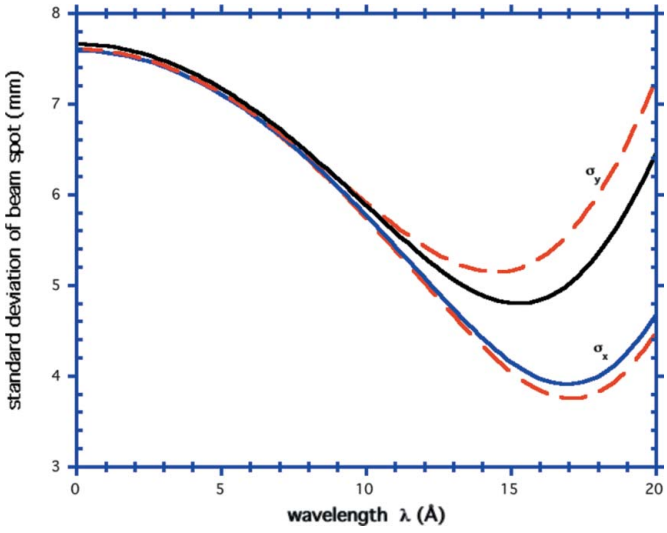

Figure 7
A comparison of the experimentally fitted standard deviation (solid lines) of the beam spot in the two directions with line-profile prediction [equations (7) and (8)] (dashed lines) as a function of wavelength. Around the focusing wavelength the experimental result for the vertical profile is better fitted with the aperture terms as in Appendix *B*.

may be a reasonable approximation to a line profile along the minor axis, the horizontal x direction. This is less so along the major axis, the vertical y direction, and is particularly poor around the optimum wavelength.

Though the beam spot center has the exact fall due to gravity as a function of λ, the fitted widths both with and without the lenses result in significantly lower values of A than those given by the beam position. Table 1 indicates the smaller than expected values for the gravity term. Furthermore, the small reduction in the vertical width when the lens aperture is increased indicates that there may be some assumption that is incorrect. On the other hand, all the horizontal beam widths are as expected. This result indicates difficulties with the chromatic term $(2/3)A^2\lambda^4(\Delta\lambda/\lambda)^2$ from the gravity contribution in (5) and (8). There may be some variation in $\Delta\lambda/\lambda$ as a function of λ and the assumption of a triangular wavelength distribution may be poor. If the distribution were described by a Gaussian of variance σ_λ^2, however, the term would be $4A^2\lambda^2\sigma_\lambda^2 = 0.721A^2\lambda^4(\Delta\lambda/\lambda)^2$, not a large difference from the assumed triangular distribution. Table 2 gives comparisons of other quantities for each of the two assumed distributions. Furthermore, the optical filter (Cook *et al.*, 2005) prior to the velocity selector has some effect on the vertical spatial-angular distribution of neutrons as a function of wavelength, giving rise to doubt regarding the validity of the assumption of uniform illumination.

We have also performed measurements without the lenses when the sample region is evacuated and compared the results when the sample region is vented. With no air scattering, the intensities are about 4% higher, with a slender increase as a function of wavelength. The x position of the beam is essentially unchanged, though the y position shifts downwards by about 0.6 mm (about 1/10 of the pixel dimension). The effect of an evacuated sample region is a small increase in transmission for the longer wavelengths, resulting in a slightly longer average wavelength. We find no change (within statistics) in the beam widths in either direction as a function of wavelength when the sample region is evacuated.

We note that our observations of the neutron optics with lenses taken on the spectrometer have no implication on small-angle measurements. Though the resolution for SANS measurements (Mildner & Carpenter, 1984) involves similar expressions, our analysis of the focused beam has greater precision, and such details that we have examined are unobservable with pixel dimensions of 5 mm in SANS measurements. Furthermore, the large uncertainty in the wavelength band of the incident beam enters at large scattering vectors where the SANS data are relatively flat, and the effect of this uncertainty remains small on the scale of the measurements.

5. Conclusions

We have performed transmission measurements on a seven-concave-lens system used for focusing the incident beam at the detector on a small-angle neutron scattering instrument, both at the focusing wavelength and as a function of wavelength. The general trends of both the beam center at the detector and the standard deviation of the breadth of the beam follow expectation.

We have analyzed the results in the thin lens approximation to the multiple lens configuration and with the assumption that the spatial distributions at the two apertures are uniform. Furthermore, we have ignored all aberrations other than the chromatic aberration, which results in beam widths varying as a function of wavelength. We have analyzed the beam width at the detector in terms of the contributions from the collimation of the experimental arrangement, from the chromatic aberration and gravity, and from the shift of the lens centerline from the spectrometer axis. These are independent and add in quadrature.

The horizontal beam width is a good measure of the spot size at the detector because it is not affected by gravity, whereas the broader vertical width results in an oval shape for the transmitted beam at the detector. Correction for this gravity effect is messy and is rarely performed for normal SANS measurements. Though single-crystal prisms can correct for the gravity effect, this effort has been motivated by

the desire to correct, at least partially, for the neutron fall by raising the lens system. We have shown that the original hypothesis is true. For equal flight paths raising our system at $\lambda = 17.2$ Å by 5 mm results in raising the beam by about 10 mm and reducing the FWHM by about 1 mm.

Full compensation occurs when $A\lambda_0^2 = w(1 + L_2/L_1)$. A symmetric beam spot is obtained when the beam is focused on the spectrometer axis at the detector, which cannot be achieved with our arrangement. Equal path lengths would require the seven-lens system to be raised 19 mm above the incident beamline for 17.2 Å neutrons. Our system could not be raised a sufficient amount, and over such long distances large and expensive lenses would be required. However, this idea can be used with a greater number of lenses and a shorter wavelength for which the neutron intensity is also more abundant. Furthermore, if the gravity term in the beam width can be understood correctly then appropriate corrections can be made to SANS data.

APPENDIX *A*
Determination of the lens transmission

Assume a concave lens of radius r, with a central aperture of radius B and a thickness $2H$ at the center. Let the macroscopic cross section be Σ at a wavelength λ. Then the transmission T of the lens averaged over the area of the aperture is given by (see Fig. 8)

$$T = (\pi B^2)^{-1} \int_0^B \exp[-2\Sigma(H + r - z)] 2\pi y \, \mathrm{d}y, \qquad (10)$$

where y is the distance of a trajectory from the optic axis and $z = (r^2 - y^2)^{1/2}$. The evaluation of this integral gives

$$T = [2(\Sigma B)^2]^{-1} \exp[-2\Sigma(H + r)]\big\{[1 - 2\Sigma(r^2 - B^2)^{1/2}] \times \exp[2\Sigma(r^2 - B^2)^{1/2}] - (1 - 2\Sigma r)\exp(2\Sigma r)\big\}, \qquad (11)$$

with the transmission for N lenses given by T^N. The fact that a trajectory makes an increasing, though small, angle to the spectrometer axis after transmission through successive lenses has a negligible effect.

Previous room-temperature measurements of the transmission of these lenses at four different wavelengths (J. G. Barker, private communication) between 5 and 20 Å have shown that the cross section may be given by Σ (mm^{-1}) = 0.000513 (13) λ (Å). We use $r = 25$ mm, $B = 6.35$ mm and $H = 0.25$ mm. The transmission calculation for seven lenses at 17.2 Å is 0.922, to be compared with the measured (including air scattering) value of 0.878, and with $[\exp(-2\Sigma H)]^7 = 0.970$ through the optic axis of the lens system. Similarly, the calculation at a wavelength of 8.4 Å for 30 lenses gives $T = 0.844$, with an experimental measurement of 0.82.

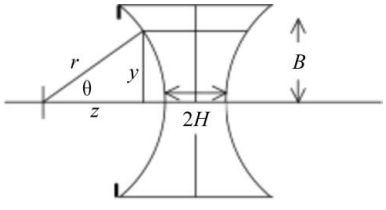

Figure 8
A schematic drawing showing how the transmission is calculated for a concave lens of radius r and a thickness $2H$ at the center, with a central aperture of radius B.

APPENDIX *B*
Determination of beam width at the detector as a function of wavelength

Not only is the beam width at the detector determined by the collimation of the experimental arrangement, but the chromaticity of the beam also affects the contributions to the transverse widths including gravity. We need to know the spatial distribution of neutrons at the detector in order to determine the FWHM of the beam at the detector for all wavelengths. This is unknown but the variance can be deduced from the distributions of neutrons at the plane of the lens and at the focal point for a given wavelength λ. Both these distributions are uniform and uncorrelated and may be used to determine the variance of the distribution on the detector plane. Note that in comparing these results with experiment, we need to add the variance from the detector pixel size, given by $(\Delta x)^2/12 = (\Delta y)^2/12$, and also to account for the averaging along a thin strip across the beam spot (this increases the theoretical variance by 4/3). We ignore any attenuation caused by the lenses themselves.

B1. Collimation contribution

The source aperture of radius R_1 placed a distance L_1 before the lens aperture is uniformly illuminated, and a uniform image is produced at a distance L_4 beyond the lens. The magnification of the source is given by $m = -(L_4/L_1)$, where the focal length f of the lens for the wavelength λ is given by the lens equation

$$1/f = 1/L_1 + 1/L_4. \qquad (12)$$

The detector plane is at a distance L_2 beyond the lens and is the image plane only for one wavelength λ_0; that is

$$1/f_0 = 1/L_1 + 1/L_2. \qquad (13)$$

The focal lengths are related by $(f/f_0) = (\lambda_0/\lambda)^2$. Hence we may write

$$1/f_0 - 1/f = (1/L_2 - 1/L_4) = (L_4 - L_2)/(L_2L_4) = 1/f_0\big[1 - (\lambda/\lambda_0)^2\big]. \qquad (14)$$

Let $\mathbf{r}_2$ and $\mathbf{r}_4$ be general points on the lens aperture of radius R_2 and on the image plane for the wavelength λ. Consider a general trajectory that passes through the points given by $\mathbf{r}_2$ and $\mathbf{r}_4$. The point at the detector $\mathbf{r}_3$ is given by (see Fig. 9)

$$\mathbf{r}_3 = (1 - L_2/L_4)(\mathbf{r}_2 - \mathbf{r}_4) + \mathbf{r}_4 = (1 - L_2/L_4)\mathbf{r}_2 + (L_2/L_4)\mathbf{r}_4. \qquad (15)$$

Since these points are uncorrelated, averaging over all points on the lens aperture and on the image plane, we obtain

$$\langle r_3^2\rangle = (1 - L_2/L_4)^2\langle r_2^2\rangle + (L_2/L_4)^2\langle r_4^2\rangle. \quad (16)$$

The image of the source aperture has a radius $(L_4/L_1)R_1$. This applies whether $L_2 < L_4$ (for $\lambda < \lambda_0$) or $L_2 > L_4$ (for $\lambda > \lambda_0$). Performing the averages gives the spatial variance at the detector

$$\sigma_r^2 = (1/2)[(L_2/L_1)^2R_1^2 + (1 - L_2/L_4)^2R_2^2]. \quad (17)$$

Using the result from equation (14) we obtain

$$\sigma_r^2 = (1/2)\left\{(L_2/L_1)^2R_1^2 + (1 + L_2/L_1)^2R_2^2[1 - (\lambda/\lambda_0)^2]^2\right\}. \quad (18)$$

The variances in each of the two perpendicular directions, σ_x^2 and σ_y^2, are equal and combine to give σ_r^2. Therefore

$$\sigma_x^2 = \sigma_y^2 = (L_2/L_1)^2(R_1/2)^2 + (1 + L_2/L_1)^2(R_2/2)^2\left[1 - (\lambda/\lambda_0)^2\right]^2. \quad (19)$$

This gives the width of the beam in the horizontal x direction at the detector as a function of wavelength. This expression clearly has a minimum at $\lambda = \lambda_0$.

This expression does not take into account the wavelength distribution of the incident beam. The value of $[1 - (\lambda/\lambda_0)^2]^2$ and other quantities averaged over both a triangular and a Gaussian wavelength distribution are given in Table 2. Hence more strictly the minimum occurs at $(\lambda/\lambda_0) = 0.991$, effectively a 0.9% decrease. Note that for the triangular wavelength distribution at $\lambda = \lambda_0$, the variance becomes

$$\sigma_x^2 = (L_2/L_1)^2(R_1/2)^2 + (1 + L_2/L_1)^2(R_2/2)^2(2/3)(\Delta\lambda/\lambda)^2. \quad (20)$$

Note also that the spatial averages are taken over the entire beam spot, whereas a line profile through the beam spot center has $(R/3^{1/2})^2$ in place of $(R/2)^2$ in the equations.

B2. Gravity contribution

We now include gravity, as well as chromatic aberration, to determine the extra width in the vertical y direction that results in the oval shape of the beam at the detector. This contribution is dependent on wavelength, and to first order is independent of changes in the trajectory direction by small angles caused by the lens. Simple kinematics shows that the change Δy in the vertical height at the detector for a beam of neutrons of a wavelength λ is given by

$$\Delta y_g = -L_2(L_1 + L_2)(g/2)(m/h)^2\lambda^2 = -A\lambda^2, \quad (21)$$

that is, the slower neutrons with the longer wavelengths fall more than the faster neutrons over a given distance.

The extra spatial variance σ_g^2 caused by gravity is therefore given by

$$\sigma_g^2 = (2/3)\,A^2\lambda^4(\Delta\lambda/\lambda)^2 = (2/3)(\Delta y)^2(\Delta\lambda/\lambda)^2. \quad (22)$$

The full expression for the width of the spot in the vertical direction at the detector is

$$\sigma_y^2 = (L_2/L_1)^2(R_1/2)^2 + (1 + L_2/L_1)^2(R_2/2)^2\left[1 - (\lambda/\lambda_0)^2\right]^2 + (2/3)A^2\lambda^4(\Delta\lambda/\lambda)^2. \quad (23)$$

This expression has a minimum approximately at

$$\lambda = \lambda_0\left[1 + (2/3)\,A^2\lambda_0^4(\Delta\lambda/\lambda)^2/(1 + L_2/L_1)^2(R_2/2)^2\right]^{-1/2}, \quad (24)$$

that is, at a wavelength that is less than λ_0. At $\lambda = \lambda_0$, the variance is given by

$$\sigma_y^2 = (L_2/L_1)^2(R_1/2)^2 + (1 + L_2/L_1)^2(R_2/2)^2(2/3)(\Delta\lambda/\lambda)^2 + (2/3)A^2\lambda_0^4(\Delta\lambda/\lambda)^2. \quad (25)$$

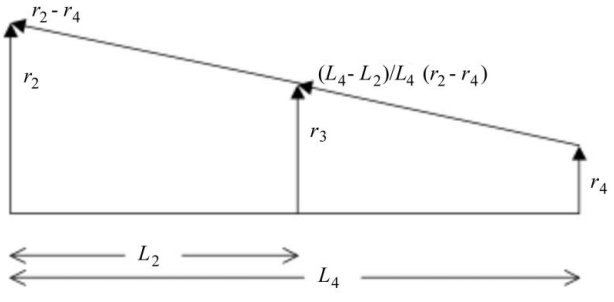

Figure 9
A schematic diagram indicating the construction of the vector $\mathbf{r}_3$ on the detector plane of the general trajectory that passes through the uncorrelated points given by the vectors $\mathbf{r}_2$ on the lens plane and $\mathbf{r}_4$ on the image plane. The detector plane and the image plane are at distances L_2 and L_4, respectively, from the lens plane.

B3. Shim contribution

We now consider those changes in the beam at the detector caused by shifting the centerline of the lens combination, in either the horizontal or the vertical direction, by a small amount using shims (see Fig. 10). An incident ray at a transverse distance $\mathbf{w}$ from, but parallel to, the centerline is redirected at the lens to pass through the focus, with a deflection angle δ as given by $\delta = |\mathbf{w}|/f$, where f is the focal length of the lens. Neglecting gravity, the refracted ray strikes the image plane at a distance $-\mathbf{w}L_4/f$ relative to the beam centerline. It also strikes the detector plane (the image plane for the wavelength λ_0) at a distance $-\mathbf{w}L_2/f_0(\lambda/\lambda_0)^2$. Therefore, as the lens system is moved using shims by a distance w, so the mean position of the beam at the detector is shifted proportionately by $-w(L_2/f_0)(\lambda/\lambda_0)^2 = -w(1 + L_2/L_1)(\lambda/\lambda_0)^2$. For $\lambda = \lambda_0$, this shift is approximately $-2w$ when $L_1 \simeq L_2 = 2f_0$.

The shift in the beam centerline in one direction has no effect on the beam in the orthogonal direction; neither the beam position nor the beam width is affected by a shim shift in the orthogonal transverse direction, so that at the wavelength $\lambda = \lambda_0$ (the wavelength corresponding to the focused position of the detector) the spatial variance is given by equation (20), which is independent of the amount of shim. For the vertical shim, on the other hand, the center of the beam spot in the y direction is raised by a distance $w(1 + L_2/L_1)$ relative to the position of the central beam for $w = 0$. Thus, the change in height of the beam center caused by gravity and by the shim for $\lambda = \lambda_0$ is given by

$$\Delta y_{gw} = -A\lambda_0^2 + w(1 + L_2/L_1). \quad (26)$$

From equation (22), the extra spatial variance caused both by gravity and by shimming is in general

$$\begin{aligned}\sigma_{gw}^2 &= (2/3)(\Delta y_{gw})^2(\Delta\lambda/\lambda)^2 \\ &= (2/3)\left[A\lambda^2 - w(1 + L_2/L_1)(\lambda/\lambda_0)^2\right]^2(\Delta\lambda/\lambda)^2 \\ &\simeq (2/3)\,A^2\lambda^4(\Delta\lambda/\lambda)^2\left[1 - 2w(1 + L_2/L_1)/(A\lambda_0^2)\right]. \quad (27)\end{aligned}$$

This results in an approximate linear decrease in the beam width in the vertical direction as a function of the shim thickness. The full spatial variance in the vertical direction including the collimation is therefore the addition of the variances of equations (19) and (27),

$$\begin{aligned}\sigma_y^2 = {} & (L_2/L_1)^2(R_1/2)^2 + (1 + L_2/L_1)^2(R_2/2)^2\left[1 - (\lambda/\lambda_0)^2\right]^2 \\ & + (2/3)A^2\lambda^4(\Delta\lambda/\lambda)^2\left[1 - 2w(1 + L_2/L_1)/(A\lambda_0^2)\right]. \quad (28)\end{aligned}$$

At $\lambda = \lambda_0$, the variance becomes

$$\begin{aligned}\sigma_y^2 = {} & (L_2/L_1)^2(R_1/2)^2 + (2/3)(1 + L_2/L_1)^2(R_2/2)^2(\Delta\lambda/\lambda)^2 \\ & + (2/3)(\Delta\lambda/\lambda)^2\left[A\lambda_0^2 - w(1 + L_2/L_1)\right]^2, \quad (29)\end{aligned}$$

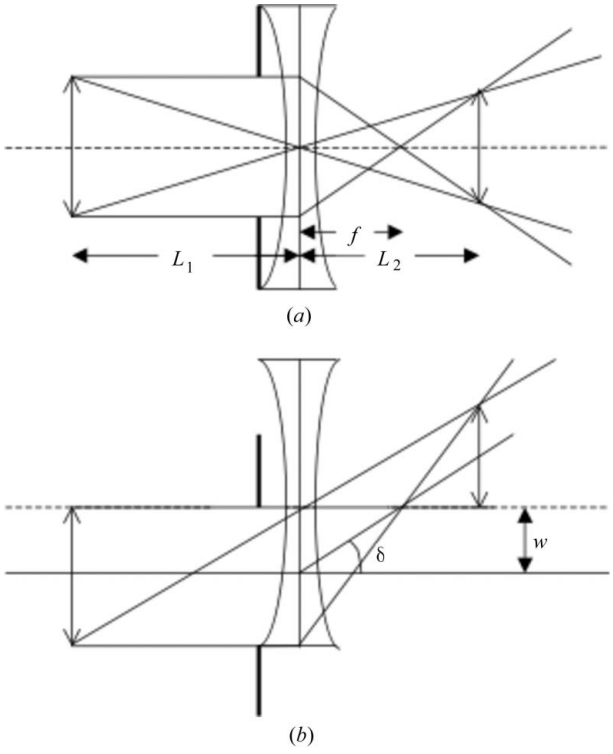

Figure 10
A diagram indicating the effect of raising the refractive lens by an amount w while keeping the aperture position stationary, for $\lambda = \lambda_0$. (*a*) The central ray is coincident with the optic axis of the lens, so that parallel rays meet at the focus, and the object has a magnification (L_2/L_1) at the image. (*b*) The central ray is a distance w below the optic axis of the lens, so that its refractive ray that passes through the focus is deflected by an angle $\delta = w/f$ relative to the optic axis. Ignoring gravity, the magnification remains the same.

which for small amounts of shim is linear in w. Interestingly, shimming the lenses to raise the beam position at the detector appears equivalent mathematically to using a slightly shorter wavelength given by

$$\lambda^2 = \lambda_0^2 - w(1 + L_2/L_1)/A. \quad (30)$$

We thank John Barker for useful discussions. This work utilized facilities supported in part by the National Science Foundation under agreement No. DMR-9986442.

References

Adachi, T., Ikeda, K., Oku, T., Sakai, K., Suzuki, S., Suzuki, J., Shimizu, H. M., Littrell, K. C., Loong, C.-K., Lin, W., Guo, J., Mitsuishi, N., Morita, S. & Ohmori, H. (2003). *J. Appl. Cryst.* **36**, 806–808.
Adachi, T., Oku, T., Morita, S., Ohmori, H., Takizawa, Y., Shimizu, H. M., Suzuki, J., Loong, C.-K., Littrell, K. C. & Goyette, R. (2002). *Appl. Phys. A*, **74**(suppl.), S180–S182.
Badurek, G., Rauch, H., Wilfing, A., Bonse, U. & Graeff, W. (1979). *J. Appl. Cryst.* **12**, 186–191.
Boothroyd, A. T. (1989). *J. Appl. Cryst.* **22**, 252–255.
Choi, S.-M., Barker, J. G., Glinka, C. J., Cheng, Y. T. & Gammel, P. L. (2000). *J. Appl. Cryst.* **33**, 793–796.
Cook, J. C., Glinka, C. J. & Schröder, I. G. (2005). *Rev. Sci. Instrum.* **76**, 025108-1–025108-8.
Eskildsen, M. R., Gammel, P. L., Isaacs, E. D., Detlefs, C., Mortensen, K. & Bishop, D. J. (1998). *Nature (London)*, **391**, 563–566.
Forgan, E. M. & Cubitt, R. (1998). *Neutron News*, **9**, 25–31.
Gähler, R., Klaus, J. & Mampe, W. (1980). *J. Phys. E Sci. Instrum.* **13**, 546–548.
Glinka, C. J., Barker, J. G., Hammouda, B., Krueger, S., Moyer, J. J. & Orts, W. J. (1998). *J. Appl. Cryst.* **31**, 430–445.
Glinka, C. J., Rowe, J. M. & LaRock, J. G. (1986). *J. Appl. Cryst.* **19**, 427–439.
Hammouda, B. (1992). *Nucl. Instrum. Methods Phys. Res. Sect. A*, **321**, 275–283.
Kentzinger, E., Dohmen, L., Alefeld, B., Rücker, U., Stellbrink, J., Ioffe, A., Richter, D. & Brückel, Th. (2004). *Physica B*, **350**, e779–e781.
Littrell, K. C. (2004). *Nucl. Instrum. Methods Phys. Res. Sect. A*, **529**, 22–27.
Mildner, D. F. R. (2005). *J. Appl. Cryst.* **38**, 488–492.
Mildner, D. F. R. & Carpenter, J. M. (1984). *J. Appl. Cryst.* **17**, 249–256.
Oku, T., Morita, S., Moriyasu, S., Yamagata, Y., Ohmori, H., Takizawa, Y., Shimizu, H. M., Hirota, T., Kiyanagi, Y., Ino, T., Furusaka, M. & Suzuki, J. (2001). *J. Nucl. Instrum. Methods Phys. Res. Sect. A*, **462**, 435–441.
Oku, T., Suzuki, J., Sasao, H., Adachi, T., Shinohara, T., Ikeda, K., Morishima, T., Sakai, K., Kiyanagi, Y., Furusaka, M. & Shimizu, H.M. (2004). *Nucl. Instrum. Methods Phys. Res. Sect. A*, **529**, 116–119.
Pantell, R. H., Feinstein J., Beguiristain, H. R., Piestrup, M. A., Gary, C. K. & Cremer, J. T. (2003). *Appl. Optics*, **42**, 719–723.
Sears, V. F. (1989). *Neutron Optics*. Oxford University Press.
Shimizu, H. M., Adachi, T., Furusaka, M., Kiyanagi, Y., Oku, T., Sasao, H., Shinohara, T. & Suzuki, J. (2004). *Nucl. Instrum. Methods Phys. Res. Sect. A*, **529**, 5–9.
Suzuki, J., Oku, T., Adachi, T., Shimizu, H. M., Hirumachi, T., Tsuchihashi, T. & Watanabe, I. (2003). *J. Appl. Cryst.* **36**, 795–799.